PRECISE DETERMINATION OF $\pi\pi$ SCATTERING AMPLITUDES FOR D AND F WAVES*

V. Nazari, Robert Kamiński

The Henryk Niewodniczański Institute of Nuclear Physics
Polish Academy of Sciences
Radzikowskiego 152, 31-342 Kraków, Poland

(Received May 18, 2015)

Precise determination of unitary multichannel $\pi\pi$ scattering amplitudes for D and F waves on the processes $\pi\pi \to \pi\pi$, $K\bar{K}$ and $\eta\eta$ in the $I^G J^{PC} = 0^+2^{++}$ and the 1^+3^{--} sectors have been presented, using a set of well known once subtracted dispersion relations with imposed crossing symmetry condition. These amplitudes were refined and re-fitted to the dispersion relations up to 1.1 GeV, and to the experimental data in the effective two-pion mass from the threshold to 2.7 GeV and 1.9 GeV for D and F waves, respectively. Moreover, a satisfactory justification regarding the controversies in the states of f_2 and ρ_3 mesons about their masses and number of states that are taken into account has been presented.

DOI:10.5506/APhysPolB.46.1355
PACS numbers: 13.25.Cq, 13.75.Lb, 11.55.Fv, 11.80.Gw

1. Introduction

To have a better understanding of strong interactions at low energies, it is crucial to have a good knowledge of light meson spectroscopy as it plays a significant role in decays that undergo strong interactions. Thus, it is very important to have model-independent information on investigated states and on their QCD nature. It can be obtained only on the basis of the first principles (analyticity and unitarity) directly applied to analysis of experimental data. This approach permits us to avoid introduction of theoretical prejudice into extracted parameters of resonances [1].

Amplitudes of $\pi\pi$ scattering are often used incorrectly. Old parameterizations of the $\pi\pi$ scattering amplitudes for D and F waves are still used in some calculations that significantly do not satisfy the crossing symmetry condition and do not describe the $\pi\pi$ threshold region. The problem

* Presented at the Cracow Epiphany Conference on the Future High Energy Colliders, Kraków, Poland, January 8–10, 2015.

is the lack of correct partial wave amplitudes for D and F waves on the processes $\pi\pi \to \pi\pi$, $K\bar{K}$ and $\eta\eta$ in the $I^GJ^{PC} = 0^+2^{++}$ and the 1^+3^{--} sectors to study the f_2 and ρ_3 mesons, respectively. Moreover, still there are some controversies in the states of f_2 and ρ_3 mesons about their masses and number of states that are taken into account. For example, in the tensor sector ($I = 2$) 0^+2^{++} from thirteen resonance states discussed in the PDG the eleven ones ($f_2(1270)$, $f_2(1430)$, $f_2(1525)$, $f_2(1600)$, $f_2(1730)$, $f_2(1810)$, $f_2(1960)$, $f_2(2000)$, $f_2(2020)$, $f_2(2240)$, $f_2(2410)$) have been confirmed in various experiments and analyses. This investigation specifies the dominant and the ineffective states.

In the analysis of S- and P-wave amplitudes [2] resonance poles and zeros on the Riemann surface that were calculated from multi-channel Breit–Wigner forms, have been used to construct the S- and P-wave amplitudes. In contrast to the way used to calculate the S- and P-wave amplitudes, multi-channel Breit–Wigner forms with taking into account the Blatt–Weisskopf barrier factors given by spins of resonances [3] have been used to construct the D- and F-wave amplitudes directly. To improve agreement of the D- and F-wave amplitudes with the crossing symmetry, the new amplitudes have been fitted to the dispersion relations (DR) and to the data.

2. The S-matrix formalism for N coupled channels

The N-channel S-matrix is determined on the 2^N-sheeted Riemann surface. The matrix elements S_{ab} ($a, b = 1, 2, \ldots, N$ denote channels) have the right-hand cuts along the real axis of the complex-s plane (s is the invariant total energy squared), related to the considered channels and starting in the channel thresholds s_i ($i = 1, \ldots, N$), and the left-hand cuts related to the crossed channels. The main model-independent part of resonance contributions is given by poles and zeros on the Riemann surface. Generally, this representation of resonances can be obtained utilizing formulas for the analytic continuations of the matrix elements for the coupled processes to the unphysical sheets of the Riemann surface [4].

For the combined analysis of data, the Le Couteur–Newton relations [5–7] have been used. These relations express the S-matrix elements of all coupled processes in terms of the Jost matrix determinant $d(k_1, \ldots, k_N)$, where the sheets of surface are numbered according to the signs of analytic continuations of the channel momenta k_i, $k_i = 1/2\sqrt{s - s_i}$ that is a real analytic function with the only branch-points at $k_i = 0$

$$S_{aa} = \frac{d(k_1, \ldots, k_{a-1}, -k_a, k_{a+1}, \ldots, k_N)}{d(k_1, \ldots, k_N)}, \tag{1}$$

$$S_{aa}S_{bb} - S_{aa}^2 = \frac{d(k_1, \ldots, k_{a-1}, -k_a, k_{a+1}, k_{b-1}, -k_b, k_{b+1}, \ldots, k_N)}{d(k_1, \ldots, k_N)}. \tag{2}$$

The real analyticity implies $d(s^*) = d^*(s)$ for all s. The d-function is taken in the separable form $d = d_{\rm bgr} d_{\rm res}$. The resonance part $d_{\rm res}$ is described using the multi-channel Breit–Wigner forms. The background part $d_{\rm bgr}$ represents mainly an influence of channels which are not explicitly included.

In the considered four-channel case, the Riemann surface is sixteen-sheeted. The sheets II, IV, VIII, and XVI correspond to the following signs of analytic continuations of the quantities: $\mathrm{Im}\sqrt{s-s_1}$, $\mathrm{Im}\sqrt{s-s_2}$, $\mathrm{Im}\sqrt{s-s_3}$, $\mathrm{Im}\sqrt{s-s_4}$: $-+++$, $+-++$, $++-+$ and $+++-$, respectively.

3. Analysis of the D-wave amplitude in the $I^G J^{PC} = 0^+2^{++}$ sector

In the analysis of data on the isoscalar D wave of processes $\pi\pi \to \pi\pi$, $K\bar{K}$ and $\eta\eta$, the channel (2π) (2π) has been considered explicitly as the fourth channel. The resonance part $d_{\rm res}$ is described using the multi-channel Breit–Wigner forms

$$d_{\rm res}(s) = \prod_r \left[M_r^2 - s - i \sum_{I=1}^{N} \rho_{ri}^{2J+1} R_{ri} f_{ri}^2 \right] , \tag{3}$$

where $\rho_{ri} = 2k_i/\sqrt{M_r^2 - s_i}$ and f_{ri}^2/M_r indicates to the partial width of a resonance with mass M_r and $R_{ri}(s, M_r, s_i, r_{ri})$ are the Blatt–Weisskopf barrier factors with s_i the channel threshold and r_{ri} a radius of the i-channel decay of the state r. The Blatt–Weisskopf barrier factor for a particle with $J = 2$ is

$$R_{ri} = \frac{9 + \frac{3}{4}\left(\sqrt{M_r^2 - s_i}\; r_{ri}\right)^2 + \frac{1}{16}\left(\sqrt{M_r^2 - s_i}\; r_{ri}\right)^4}{9 + \frac{3}{4}\left(\sqrt{s - s_i}\; r_{ri}\right)^2 + \frac{1}{16}\left(\sqrt{s - s_i}\; r_{ri}\right)^4} , \tag{4}$$

with radii r_{ri} 0.943 fm for resonances in all channels, except for $f_2(1270)$ and $f_2(1960)$ for which the radii are: for $f_2(1270)$, 1.498, 0.708, and 0.606 fm in channels $\pi\pi$, $K\bar{K}$ and $\eta\eta$, respectively, and for $f_2(1960)$, 0.296 fm in the $K\bar{K}$ channel. The background part has the form

$$d_{\rm bgr} = \exp\left[-i \sum_{i=1}^{3} \left(\sqrt{\frac{s - s_n}{s}} \right)^5 (a_n + i b_n) \right] , \tag{5}$$

where

$$a_1 = \alpha_{11} + \frac{s - 4m_K^2}{s}\; \alpha_{12}\; \theta\left(s - 4m_K^2\right) + \frac{s - s_v}{s}\; \alpha_{10}\; \theta(s - s_v) , \tag{6}$$

$$b_n = \beta_n + \frac{s - s_v}{s}\ \gamma_n\ \theta(s - s_v)\,, \tag{7}$$

where α_{11}, α_{12}, α_{10}, β_n and γ_n are background parameters, and $s_v = 4m_v^2$ ($m_v = 759$) is a combined threshold of the channels $\eta\eta'$, $\rho\rho$, and $\omega\omega$.

The data for the $\pi\pi$ scattering are taken from an energy-independent analysis by Hyams *et al.* [8]. The data for $\pi\pi \to K\bar{K}$, $\eta\eta$ are taken from works in Ref. [9]. The parameters of the Breit–Wigner generators of the poles are shown in Table I.

TABLE I

The parameters of the Breit–Wigner forms for 11 f_2-states (in MeV).

State	M_r	f_{r1}	f_{r2}	f_{r3}	f_{r4}
$f_2(1270)$	1276.3 ± 13	468.9 ± 34.2	201.6 ± 45.4	89.9 ± 11.4	7.2 ± 4.76
$f_2(1430)$	1534.7 ± 38	28.5 ± 11.7	253.9 ± 94.2	89.4 ± 14.5	51.6 ± 21.3
$f_2(1525)$	1760 ± 12.4	129.5 ± 51.3	259 ± 108.4	469.7 ± 55.3	90.3 ± 32.2
$f_2(1600)$	1450.5 ± 98	128.3 ± 10.8	562.3 ± 99.2	32.7 ± 17.9	8.2 ± 1.2
$f_2(1730)$	1719.8 ± 98	78.8 ± 19.3	289.5 ± 38.9	460.3 ± 98.1	108.6 ± 28.3
$f_2(1810)$	1962.2 ± 48	132.6 ± 74.8	331 ± 162.2	319 ± 57.8	62.4 ± 33.6
$f_2(1960)$	1601.5 ± 68	75.5 ± 47.8	315 ± 246.7	388.9 ± 91.5	127 ± 36.8
$f_2(2000)$	2202.0 ± 47	133.4 ± 15.3	545 ± 34.24	381 ± 25.72	168.8 ± 34.6
$f_2(2020)$	2006 ± 35.1	155.7 ± 91.4	169.5 ± 51.8	60.4 ± 13.83	168.8 ± 74.8
$f_2(2240)$	2387 ± 62.3	175 ± 61.4	395 ± 87.2	24.5 ± 15.7	462.8 ± 92.1
$f_2(2410)$	2027 ± 150	50.4 ± 11.2	441 ± 116.9	58 ± 12.5	128 ± 34.82

The background parameters are: $\alpha_{11} = -0.0755$, $\alpha_{12} = 0.0225$, $\alpha_{10} = -0.2344$, $\beta_1 = -0.0782$, $\beta_2 = -0.985$, $\beta_3 = -0.5162$, $\gamma_1 = -0.05215$, $\gamma_2 = 0.7494$ and $\gamma_3 = 0.786$.

4. Analysis of the *F*-wave amplitude in the $I^G J^{PC} = 1^+3^{--}$ sector

The dominant modes of decay of the $\rho_3(1690)$ are $\pi\pi$, 4π, $\omega\pi$ and $K\bar{K}$ that are taken into account in analysis of the $\pi\pi$ scattering data in the $I^G J^{PC} = 1^+3^{--}$ sector by Hyams *et al.* [8] and therefore have used the four-channel Breit–Wigner forms in constructing the Jost matrix determinant $d\,(\sqrt{s - s_1}, \sqrt{s - s_2}, \sqrt{s - s_3}, \sqrt{s - s_4})$, where $s_1, \ldots, s_4$ are respectively the thresholds of the first four channels given above. For the combined analysis of data, the Le Couteur–Newton relations [5–7] have been used. These relations express the S-matrix elements of all coupled processes in terms of the Jost matrix determinant as below

$$S_{11} = \frac{d\,(-\sqrt{s - s_1}, \ldots, \sqrt{s - s_4}\,)}{d\,(\sqrt{s - s_1}, \ldots, \sqrt{s - s_4}\,)}\,. \tag{8}$$

The resonance part of the d-function Eq. (3) has the form

$$d_{\rm res}(s) = \prod_r \left[M_r^2 - s - i \sum_{j=1}^{4} \left(\sqrt{\frac{s - s_j}{M_r^2 - s_j}} \right)^7 R_{rj} f_{rj}^2 \right] . \tag{9}$$

The Blatt–Weisskopf factor for a particle with $J = 3$ is

$$R_{rj} = \frac{15+3\left(\sqrt{M_r^2 - s_j}\; r_{rj}\right)^2 + \frac{2}{5}\left(\sqrt{M_r^2 - s_j}\; r_{rj}\right)^4 + \frac{1}{15}\left(\sqrt{M_r^2 - s_j}\; r_{rj}\right)^6}{15 + 3\left(\sqrt{s - s_j}\; r_{rj}\right)^2 + \frac{2}{5}\left(\sqrt{s - s_j}\; r_{rj}\right)^4 + \frac{1}{15}\left(\sqrt{s - s_j}\; r_{rj}\right)^6} \tag{10}$$

with radii $r_{rj} = 0.927$ fm in all channels. The background part is

$$d_{\rm bgr} = \exp\left[-i \left(\sqrt{\frac{s - 4m_\pi^2}{s}} \right)^7 (\alpha_n + i\beta_n) \right] , \tag{11}$$

where α_n and β_n are background parameters. Values of α_1 and β_1 are -0.0127 and 0.0067 respectively, and α_2, α_3, β_3 and β_3 are fixed at zero. In the analysis, cases with one and two resonances, namely $\rho_3(1690)$ and $\rho_3(1950)$, have been considered.

The parameters of the Breit–Wigner generators of the poles are shown in Table II. One can also calculate position of the poles using these parameters.

TABLE II

Mass and total width of the $\rho_2(1690)$, $\rho_2(1950)$ and their branching ratios compared with the average values from the PDG Tables (in MeV).

State	M_r	f_{r1}	f_{r2}	f_{r3}	f_{r4}
$\rho_3(1690)$	1707.8 ± 13.7	284.4 ± 15.9	435.3 ± 21.0	208.6 ± 18.4	113.5 ± 25
$\rho_3(1950)$	1833.5 ± 28	96.3 ± 18.3	331.8 ± 28.0	297.7 ± 16.5	110.4 ± 28.3

5. Multichannel amplitudes and dispersion relations

Having matrix element S_{11} from Eqs. (1) and (8), one can calculate the full amplitudes $f_\ell^I(s)^{\rm in}$ for given isospin I and spin ℓ

$$f_\ell^I(s)^{\rm in} = \frac{\sqrt{s}}{2k} \frac{S_{11} - 1}{2i} , \tag{12}$$

where $k = \sqrt{s/4 - M_\pi^2}$ and M_π is the pion mass.

In order to obtain a precise description of $\pi\pi$ amplitudes, GKPY dispersion relations [10, 11] with imposed crossing symmetry have been applied to the D- and F-wave amplitudes. These new dispersion relations should impose quite strong constraints in the fits to the data on the analyzed $\pi\pi$ interactions. Hence,

$$\mathrm{Re} f_\ell^I(s)^{\mathrm{out}} = \sum_{I'=0}^{2} C_{st}^{II'} a_0^{I'} + \sum_{I'=0}^{2}\sum_{\ell'=0}^{3} \oint_{4m_\pi^2}^{S_{\max}} ds' K_{\ell\ell'}^{II'}(s,s') \mathrm{Im} f_{\ell'}^{I'}(s')^{\mathrm{in}} + d_\ell^I(s)\,. \tag{13}$$

Given $f_\ell^I(s)$ amplitude fulfills the crossing symmetry when real part of the output amplitude $\mathrm{Re}\, f_\ell^I(s)^{\mathrm{out}}$ is equal to real part of the input one $\mathrm{Re}\, f_\ell^I(s)^{\mathrm{in}}$. The angular momentum ℓ' of the input amplitudes goes from 0 to 3 (the S, P , D and F waves) and because of the Bose symmetry, the sums $\ell' + I'$ and $\ell + I$ for input and output amplitudes respectively, must be even (see Ref. [12] for more details).

In order to check how the D- and F-wave amplitudes described in Secs. 3 and 4 fulfill the crossing symmetry condition, one has to use them as the input amplitudes in Eq. (13), *i.e.* integrate their imaginary parts with proper kernels from the threshold to 1.42 GeV. However, as it is shown in Fig. 1, clearly one sees an inappropriate behavior of phase shifts (original) near the $\pi\pi$ threshold. These amplitudes have to be re-defined in the vicinity of the $\pi\pi$ threshold. Therefore, in order to allow the integration from the $\pi\pi$ threshold, the D-wave amplitude has been re-defined for energies $\sqrt{s_{\mathrm{th}}} < \sqrt{s} < \sqrt{s_{02}}$, where $\sqrt{s_{02}}$ is matching energy for the D wave and $\sqrt{s_{\mathrm{th}}}$ is the $\pi\pi$ threshold. Above this energy, the amplitude remains fully equivalent to the "original" multichannel one from Sec. 3. Below this energy, the amplitude is parameterized as

$$\sin 2\delta_2^0 = \frac{4m_\pi k^5}{\sqrt{s}} \left[a_2^0 + b_2^0 k^2 + c_2^0 k^4 + d_2^0 k^6 + \mathcal{O}\left(k^8\right)\right]. \tag{14}$$

In Eq. (14), the parameters a_2^0 and b_2^0 are the scattering length and the so-called slope parameter respectively, which can be fixed or fitted to the data and to the dispersion relations. In this analysis, they were fixed at the values: $a_2^0 = 0.00178\ m_\pi^{-5}$ and $b_2^0 = 0.00035\ m_\pi^{-7}$. The parameters c_2^0 and d_2^0 are calculated from the continuity conditions for the phase shifts and their first derivatives at the matching energy to match smoothly the phase shift Eq. (14) with the multichannel "original" one from Sec. 3 at the matching energy $\sqrt{s_{02}}$. Figure 1 (left) shows how the extended amplitude solved the threshold behavior problem of low-energy D wave $\pi\pi$ interaction amplitude and value of the matching energy $\sqrt{s_{02}}$ was found to be 752.

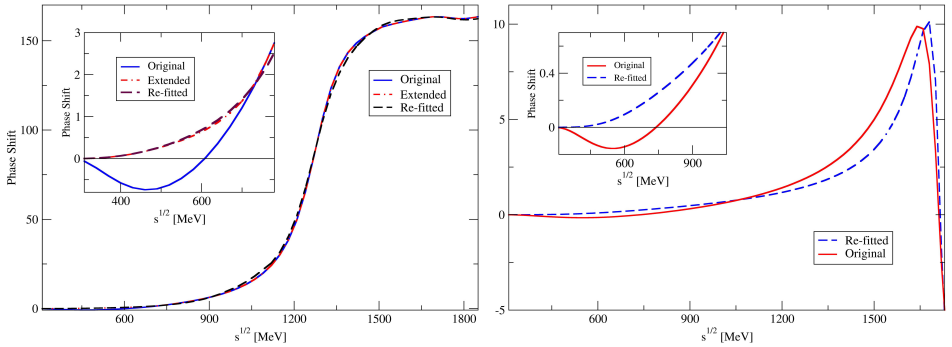

Fig. 1. Phase shifts for the D- (left) and the F- (right) wave amplitudes as a function of energy for the original (solid line), extended (dash-dotted line) and re-fitted (dashed line) amplitudes considered in the text from threshold up to 1.8 GeV.

To refine the F-wave amplitude in the vicinity of $\pi\pi$ threshold, another way of refining has been applied. To refine this part, some pseudo-date have been generated from $\pi\pi$ threshold up to 895 MeV using GKPY equations to uplift the phase shift.

6. Results of refining

The partial waves are considered to be fully independent in the multichannel analysis. Now, to improve agreement of the $D0$- and $F1$-wave amplitudes with the crossing symmetry, the extended amplitudes have been fitted to the GKPY dispersion relations and to the data, where for the D wave the $S0$, $S2$, $P1$, $D2$ and $F1$ and, for the F wave the $S0$, $S2$, $P1$, $D0$ and $D2$ have been taken from [10] and fixed. Hence, the total χ^2 was composed of five parts for D wave and six parts for F wave

$$\chi^2 = \chi^2_{\text{Data}} + \sum_{j=1}^{n} \chi^2_{\text{DR}}(j)\,, \tag{15}$$

where $n = 4$ is for the $S0$, $S2$, $P1$ and $D0$ partial waves for the D wave, and $n = 5$ is for the $S0$, $S2$, $P1$, $D0$ and $F1$ partial waves for the F wave, respectively. Corresponding χ^2_{Data} and $\chi^2_{\text{DR}}(j)$ are expressed by

$$\chi^2_{\text{Data}} = \frac{\left(\delta_i^{\text{exp}} - \delta_i^{\text{th}}\right)^2}{\left(\Delta\delta_i^{\text{exp}}\right)^2} + \frac{\left(\eta_i^{\text{exp}} - \eta_i^{\text{th}}\right)^2}{\left(\Delta\eta_i^{\text{exp}}\right)^2} \tag{16}$$

and

$$\chi^2_{\text{DR}}(j) = \sum_{i=1}^{N_{\text{DR}}} \frac{\left[\text{Re} f_\ell^I(s_i)^{\text{out}} - \text{Re} f_\ell^I(s_i)^{\text{in}}\right]^2}{\left[\Delta_{\text{DR}}\right]^2}\,. \tag{17}$$

Symbols δ_i and η_i denote experimental and calculated values of the phase shift and inelasticity parameter in the assumed channels of the D wave (F wave) in all considered channels and with corresponding errors Δ. $N_{\rm DR}$ for DR was chosen to be 26 for each fitted partial wave to cover the $m_{\pi\pi}$ range from 0.31 GeV to 1.09 GeV with step 0.03 GeV. The output amplitudes $\mathrm{Re} f_\ell^I(s_i)^{\rm out}$ in Eq. (17) are calculated using the GKPY equations (13) and their errors ($\Delta_{\rm DR}$) are fixed at 0.01. Note that, the input amplitudes $\mathrm{Re}\, f_\ell^I(s_i)^{\rm in}$ come directly from the extended amplitudes and other input amplitudes are taken from Ref. [10].

6.1. Results of the analysis for D wave

The total number of data points $N_\delta^{D0}+N_\eta^{D0}$ is 199. The free parameters considered in the $D0$ wave are: the background parameters in the elastic channel α_{11}, α_{12}, α_{10}, β_1, β_2, β_3, γ_1, γ_2 and γ_3, the matching energy $\sqrt{s_{02}}$ and parameters of the states $f_2(1270)$, $f_2(1430)$, $f_2(1525)$ and $f_2(1600)$. Therefore, the total number of free parameters is 30.

Table III shows values of the total χ^2 and its contributions from the data and the dispersion relations along with the χ^2 per number of degrees of freedom χ^2/n.d.f. before (extended) and after (re-fitted) fitting. (n.d.f. $= 199+104-30$).

TABLE III

Values of the χ^2 for the extended (before fitting) and re-fitted (after fitting) D-wave amplitude.

	χ^2	$\chi^2_{\rm Data}$	$\chi^2_{\rm DR}$	χ^2/n.d.f.
Extended	1129.35	758.08	371.267	4.14
Re-fitted	409.84	270.76	139.08	1.50

Figure 2 illustrates real parts of input and output of the extended and re-fitted amplitudes for $D0$ wave. However, extended amplitude does not fulfill the crossing symmetry condition yet. A big difference is very well seen between the real parts of the input and output amplitudes. Effect of the crossing symmetry condition is also seen very well in Fig. 2 (right) below about re-fitted matching energy *i.e.* 907 MeV where unsuitable behavior of amplitude have been solved.

Concerning the dominant and the ineffective states in the multichannel analysis on the processes $\pi\pi\to\pi\pi$, $K\bar{K}$ and $\eta\eta$ in the $I^GJ^{PC}=0^+2^{++}$ sector, several fits have been performed. Table IV shows values of the χ^2 for different fits with neglected states. Nevertheless, conditions are the same for all fits and they just differ by the neglected states. Values of the χ^2

achieved through fits 1, 2, 3 and 6 are almost equal. From the point of view of χ^2, one can neglect the states $f_2(2240)$ and $f_2(2410)$, and conclude that these two states are negligible on the processes $\pi\pi \to \pi\pi$, $K\bar{K}$ and $\eta\eta$ in the $I^G J^{PC} = 0^+2^{++}$ sector. Additionally, states $f_2(1270)$, $f_2(1430)$, $f_2(1525)$ and $f_2(1600)$ which strongly influence the behavior of the amplitude and consequently value of the χ^2 are the dominant states.

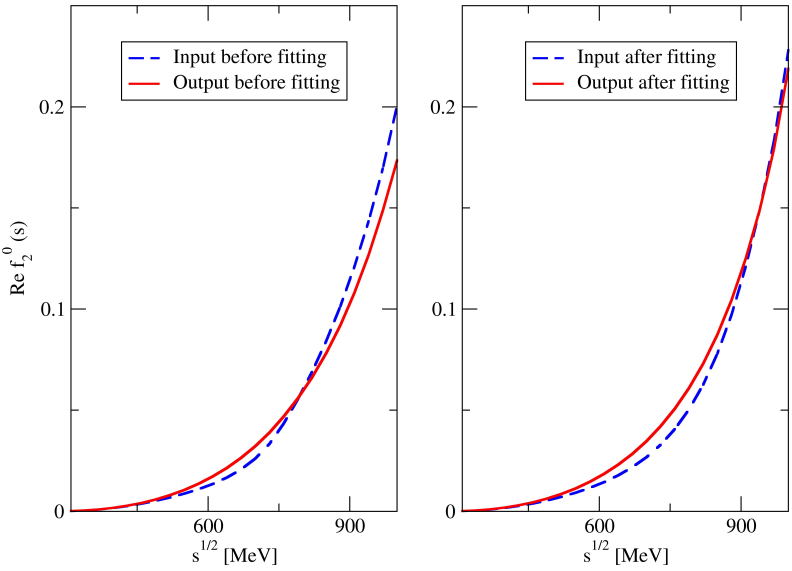

Fig. 2. Real parts of input and output of the $D0$ amplitude before (left) and after (right) fitting.

TABLE IV

Values of χ^2 when some of the states are neglected in the $I^G J^{PC} = 0^+2^{++}$ sector after fitting.

Fit No.	Neglected states	χ^2
1	All stated are included	409.8
2	$f_2(2240)$	409.7
3	$f_2(2410)$	409.4
4	$f_2(2000)$	429.5
5	$f_2(1810)$	419.1
6	$f_2(2240)$ $f_2(2410)$	409.9
7	$f_2(2240)$ $f_2(2410)$ $f_2(2000)$	439.8
8	$f_2(2240)$ $f_2(2410)$ $f_2(2000)$ $f_2(1810)$	442.9

6.2. Results of the analysis for F wave

The total number of data points $N_\delta^{F1} + N_\eta^{F1}$ is 108. The free parameters considered in the $F1$ wave are: the background parameters in the elastic channel α_1 and β_1 and five parameters of the state $\rho_3(1690)$.

Table V shows values of the total χ^2 and its contributions from the data and the dispersion relations along with the χ^2 per number of degrees of freedom for several fits. Table VI shows values of the M_r for $\rho_3(1690)$ and $\rho_3(1950)$ states before and after fitting which gives us significant information about masses of the states in all possible fits.

TABLE V

Values of the χ^2 for the re-fitted (after fitting) F-wave amplitude for all possible choices.

Fit No.	Free states	Neglected states	n.d.f.	χ^2_{Data}	χ^2_{DR}	χ^2	χ^2/n.d.f.
F_a	$\rho_3(1690)$	—	226	380.19	140.22	520.40	2.30
F_b	$\rho_3(1950)$	—	226	542.18	151.33	693.51	3.07
F_c	$\rho_3(1690)$, $\rho_3(1950)$	—	221	366.73	139.71	506.43	2.29
F_d	$\rho_3(1690)$	$\rho_3(1950)$	226	366.24	139.84	506.08	2.24
F_e	$\rho_3(1950)$	$\rho_3(1690)$	226	366.34	139.84	506.18	2.24

TABLE VI

Values of the M_r for $\rho_3(1690)$ and $\rho_3(1950)$ states before and after fitting for F-wave amplitude. For neglected states, the initial value of the mass changed to 30000 at the beginning.

Fit No.	$\rho_3(1690)$ Initial $\to$ Final	$\rho_3(1950)$ Initial $\to$ Final
F_a	1710.7 $\to$ 1713.8	1833.5 $\to$ 1833.5
F_b	1710.7 $\to$ 1710.7	1833.5 $\to$ 11286
F_c	1710.7 $\to$ 1716.1	1833.5 $\to$ 5032.7
F_d	1710.7 $\to$ 1715.9	30000 $\to$ 30000
F_e	30000 $\to$ 30000	1833.5 $\to$ 1715.9

Looking at the re-fitted masses of the states $\rho_3(1690)$ and $\rho_3(1950)$ in Table VI, it is clearly seen that, when parameters of the state $\rho_3(1950)$ are free, mass of the state $\rho_3(1690)$ must be either neglected at the beginning or becomes very big after fitting. Therefore, fits F_b, F_c and F_e, where parameters of the $\rho_3(1950)$ state are taken to be free, are not appropriate. One can conclude that both fits F_a and F_d are plausible although χ^2 of the fit F_d is smaller than the one in the fit F_a.

Figure 3 illustrates real parts of input and output of the extended and re-fitted amplitudes for $F1$ wave. However, extended amplitude does not fulfill the crossing symmetry condition yet. The effect of the crossing symmetry condition is very well seen particularly below about 900 MeV where some pseudo-data were added.

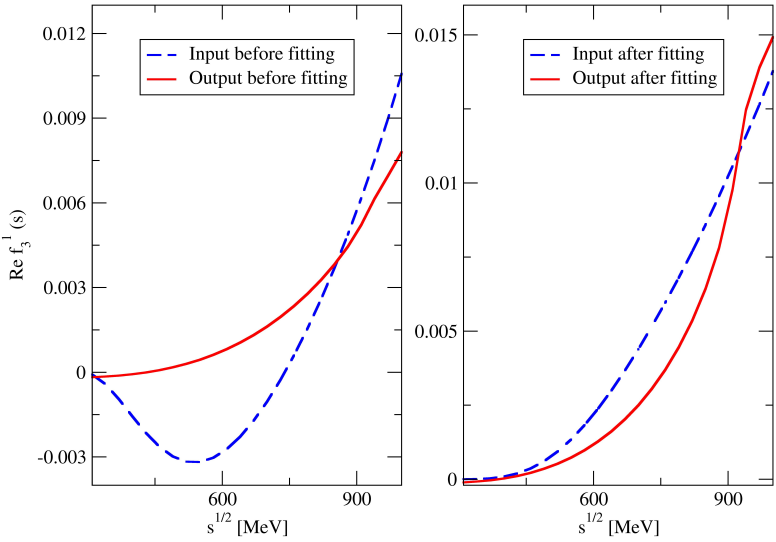

Fig. 3. Real parts of input and output of the $F1$ amplitude before (left) and after (right) fitting.

6.3. Results of the analysis for D and F waves

The D- and F-wave amplitudes have been precisely determined separately in Secs. 6.1 and 6.2 using the dispersion relations with imposed crossing symmetry condition. However, the D- and F-wave amplitudes intuitively correlate with each other in kernel term of Eq. (13). Therefore, to improve agreement of the $D0$- and $F1$-wave amplitudes with the crossing symmetry, the re-fitted amplitudes of D and F waves have been fitted to the GKPY dispersion relations and to the data, where the $S0$, $S2$, $P1$ and $D2$ have been taken from [10] and fixed. Consequently, the total χ^2 was composed of six parts

$$\chi^2 = \sum_{j=1}^{2} \chi^2_{\mathrm{Data}}(j) + \sum_{j'=0}^{3} \chi^2_{\mathrm{DR}}\left(j'\right) \ , \tag{18}$$

where $j = 1, 2$ itemizes the D and F partial waves respectively, and $j' = 0, \ldots, 3$ itemizes all partial waves. Table VII shows values of the χ^2 for the D- and F-wave amplitudes after fitting using results of the re-fitted D- and F-wave amplitudes in Secs. 6.1 and 6.2.

TABLE VII

Values of the χ^2 for the D- and F-wave amplitudes after fitting. $DF_a(DF_d)$ is the fit using fitted parameters of D wave and, $F_a(F_d)$ for F wave as initial values.

Fit No.	$\chi^2_{\rm Data}(D)$	$\chi^2_{\rm Data}(F)$	$\chi^2_{\rm DR}$	χ^2	χ^2/n.d.f.
DF_a	252.7	379.8	128.9	761.5	1.90
DF_d	257.7	366.4	129.4	753.6	1.88

7. Conclusions

To conclude, the new re-fitted multichannel D and F wave $\pi\pi$ scattering amplitudes on the processes $\pi\pi \to \pi\pi$, $K\bar{K}$ and $\eta\eta$ in the $I^G J^{PC} = 0^+2^{++}$ and the 1^+3^{--} sectors have been precisely determined. New amplitudes fulfilled crossing symmetry and describe the $\pi\pi$ threshold region very well. The dominant and the ineffective states of 0^+2^{++} and 1^+3^{--} sectors have been specified.

This work has been funded by the Polish National Science Centre (NCN) Grant No. DEC-2013/09/B/ST2/04382.

REFERENCES

[1] S. Godfrey, N. Isgur, *Phys. Rev. D* **32**, 189 (1985).
[2] P. Bydžovský, R. Kamiński, V. Nazari, *Phys. Rev. D* **90**, 116005 (2014).
[3] J. Blatt, V. Weisskopf, *Theoretical Nuclear Physics*, Wiley, NY 1952.
[4] D. Krupa, V.A. Meshcheryakov, Yu.S. Surovtsev, *Nuovo Cim. A* **109**, 281 (1996).
[5] K.J. Le Couteur, *Proc. Roy. Soc. A* **256**, 115 (1960).
[6] R.G. Newton, *J. Math. Phys.* **2**, 188 (1961).
[7] M. Kato, *Ann. Phys.* **31**, 130 (1965).
[8] S.D. Protopopescu *et al.*, *Phys. Rev. D* **7**, 1279 (1973); B. Hyams *et al.*, *Nucl. Phys. B* **64**, 134 (1973); P. Estabrooks, A.D. Martin, *Nucl. Phys. B* **79**, 301 (1974).
[9] S.J. Lindenbaum, R.S. Longacre, *Phys. Lett. B* **274**, 492 (1992); R.S. Longacre *et al.*, *Phys. Lett. B* **177**, 223 (1986).
[10] R. García-Martín *et al.*, *Phys. Rev. D* **83**, 074004 (2011).
[11] R. Kamiński, *Phys. Rev. D* **83**, 076008 (2011).
[12] V. Nazari, P. Bydžovský, R. Kamiński, *Acta Phys. Pol. B* **45**, 1549 (2014).